Ocean Dynamics (2004) 54: 54–65
DOI 10.1007/s10236-003-0065-4

Rezwan Mohammad · Johan Nilsson

The role of diapycnal mixing for the equilibrium response of thermohaline circulation

Received: 8 May 2003 / Accepted 7 October 2003

Abstract Using a zonally averaged, one-hemispheric numerical model of the thermohaline circulation, the dependence of the overturning strength on the surface equator-to-pole density difference is investigated. It is found that the qualitative behavior of the thermohaline circulation depends crucially on the nature of the small-scale vertical mixing in the interior of the ocean. Two different representations of this process are considered: constant vertical diffusivity and the case where the rate of mixing energy supply is taken to be a fixed quantity, implying that the vertical diffusivity decreases with increasing stability of the water column. When the stability-dependent diffusivity parameterization is applied, a weaker density difference is associated with a stronger circulation, contrary to the results for a fixed diffusivity. A counterintuitive consequence of the stability-dependent mixing is that the poleward atmospheric freshwater flux, which acts to reduce the thermally imposed density contrast, strengthens the thermally dominated circulation and its attendant poleward heat transport. However, for a critical value of the freshwater forcing, the thermally dominated branch of steady states becomes unstable, and is succeeded by strongly time-dependent states that oscillate between phases of forward and partly reversed circulation. When a constant vertical diffusivity is employed, on the other hand, the thermally dominated circulation is replaced by a steady salinity-dominated state with reversed flow. Thus in this model, the features of the vertical mixing are essential for the steady-state response to freshwater forcing as well as for the character of flow that is attained when the thermally dominated circulation becomes unstable.

Responsible Editor: Jin-Song von Storch

R. Mohammmad (✉) · J. Nilsson
Department of Meteorology,
Stockholm University,
106, 91 Stockholm, Sweden
e-mail: Rezwan.Mohammad@misu.su.su

Keywords Thermohaline circulation · Stability · Vertical mixing · Numerical modeling · Scale theory

1 Introduction

The view that freshwater forcing, associated with the meridional atmospheric transport of water vapor, curtails and destabilizes the thermohaline circulation is deeply rooted inside as well as outside the scientific community. The argument behind this notion is straightforward and based on two considerations; pro primo, the fact that the freshwater forcing creates a salinity field that reduces the thermally imposed equator to pole-density difference and pro secundo, the assumption that the thermohaline circulation is favored by a strong equator-to-pole density difference. Furthermore, this view seems to be supported by the results from a large body of numerical ocean-circulation studies (e.g., Marotzke et al. 1988; Weaver et al. 1993; Park and Bryan, 2000).

Contrary to established wisdom, however, a number of recent investigations (Lyle 1997; Huang 1999; Nilsson and Walin, 2001) have concluded that it is fully possible that the thermohaline circulation may intensify, rather than slow down, in response to a weaker equator-to-pole density difference. The relation between vertical mixing and the stratification is at the heart of this remarkable result, and the underlying physics are straightforward. Consider thermohaline circulation in a one-hemisphere basin, where a thermocline separates the warm poleward-flowing water in the upper ocean from the cold water beneath. Suppose now that the equator-to-pole density difference suddenly is reduced and that the ocean adjusts to the new forcing. Regardless of the details of vertical mixing, we will observe two changes after the adjustment; the speed of the poleward-flowing warm water has decreased, and the depth of the thermocline has increased. The latter change serves to augment the net poleward flow, whereas the former acts to hamper it. It is here that the properties of vertical mixing, which controls the response of thermocline depth, become crucial: if the

turbulent vertical diffusivity is assumed to be fixed – the standard assumption in ocean modeling – the net poleward flow will decline. On the other hand, if the diffusivity increases as the stratification becomes weaker – a physically reasonable behavior – the net poleward transport may amplify. Based on these considerations, Nilsson and Walin (2001) advanced the idea that the reduction in the equator-to-pole density difference caused by the salinity field may serve to strengthen the thermohaline circulation, rather than to weaken it.

In fact, the numerical one-hemisphere simulations due to Huang (1999) and Nilsson et al. (2003b) have demonstrated that if the vertical mixing is suppressed by strong stratification, the strength of thermohaline circulation decreases with increasing equator-to-pole density difference. Both these studies dealt with purely thermal flows, forced by a prescribed distribution of sea-surface temperature. However, when the circulation is forced by a prescribed sea-surface temperature as well as by a freshwater flux (i.e., mixed boundary conditions), the surface density distribution becomes a function of the flow. As pointed out by Stommel (1961), this implies that there may exist multiple equilibria. In addition to the thermally dominated circulation of the forward type – the mode studied by Huang (1999) and Nilsson et al. (2003b) – there generally exist equilibria with reversed flow where the salinity field dominates the density distribution (e.g., Welander 1986; Thual and McWilliams 1992; Weaver et al. 1993). Further, there may exist an upper bound on the freshwater forcing, beyond which an equilibrium with forward circulation cannot be attained.

A main purpose of the present study is to explore how the representation of vertical mixing affects the overturning dynamics when the circulation is forced by mixed boundary conditions. To address this issue, a two-dimensional numerical model has been employed and simulations have been carried out for a broad range of surface forcing. The model is a zonally averaged representation of thermohaline circulation in a single-hemisphere basin. As a preliminary to the numerical investigation, a scale analysis of thermohaline flows is presented. Basically, this analysis follows that of Nilsson and Walin (2001). However, a theoretical investigation of the dynamics in the limit where the thermocline depth approaches the ocean bottom represents a novel contribution, an issue followed up in the analyses of the numerical simulations. It is emphasized that this is an idealized study addressing a problem of basic importance for the dynamics of the thermohaline circulation. As with all idealized models, there are caveats associated with this study. Thus in the concluding section, the relevance of our findings for the real ocean are subjected to a critical discussion.

2 Scaling analysis

Our first step is to apply a simple scale analysis to the thermohaline circulation in order to judge how its

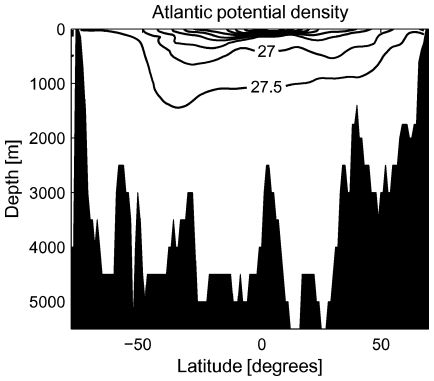

Fig. 1 Meridional potential density cross-section in the Atlantic basin along 30° west latitude. Density in units of kg m^{-3} − 1000. Contour interval is 0.5 kg m^{-3}. (Data from Levitus 1982)

strength is related to the equator-to-pole density difference and the specifics of the vertical mixing. As background it is instructive to consider a meridional cross-section of potential density distribution in the Atlantic basin (cf. Fig. 1). These observations suggest that, as a first approximation, the ocean may be regarded as stratified where a thin upper layer of light water is separated from a deep, nearly homogeneous layer of dense water by a pycnocline. Furthermore, the observations indicate that the equator-to-pole density difference at the surface to lowest order equals the vertical density difference at low latitudes.

In what follows a one-hemispheric basin is considered[1] (cf. Fig. 2). The equator-to-pole density difference at the surface ($\Delta\rho$) is prescribed, whereas the depth of the pycnocline (H) and the circulation (ψ) are to be predicted. The depth of the basin is denoted D, the poleward volume transport is ψ_{I}, and the diapycnal volume transport upwards is ψ_{II}. Here, the depth of the pycnocline is assumed to be small, $H/D \ll 1$. (The case when the pycnocline depth is large, $H \sim D$, is dealt with separately.)

In the scale analysis the circulation is assumed to be in hydrostatic and geostrophic balance, which implies (Welander 1986) that the thermal wind relation is valid:

$$\frac{\partial v}{\partial z} = -\frac{g}{f\rho_0}\cdot\frac{\partial \rho}{\partial x} \quad .$$

Here, x and z are the independent coordinates in the zonal and vertical directions, respectively, v is the meridional velocity, g the gravity, f the Coriolis parameter, ρ the density, and ρ_0 a reference density. Furthermore, vertical advection is assumed to balance vertical diffusion (Munk 1966):

$$w\frac{\partial \rho}{\partial z} = \frac{\partial}{\partial z}\left(\kappa\frac{\partial \rho}{\partial z}\right) \quad ,$$

[1] Here, the one-hemisphere geometry may be viewed as a conceptual representation of a general thermohaline flow where the low-latitude upwelling is routed towards the sinking regions in near-surface currents; see also the discussion in the concluding section.

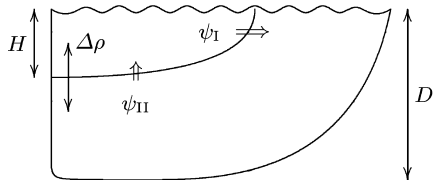

Fig. 2 Sketch of a simple one-hemisphere two-layer system

where w is the vertical velocity and κ is the diffusivity coefficient representing the vertical small-scale mixing.

To estimate the overturning circulation, the poleward and diapycnal flows have to be determined. The former quantity is scaled using the thermal wind relation, where the zonal density gradient is assumed to be proportional to that in the meridional direction, a conjecture which is supported by results from three-dimensional modeling (e.g., Wright and Stocker 1991: Wright et al. 1989; Park and Bryan, 2000). This proportionality implies that the poleward volume transport scales as

$$\psi_{\mathrm{I}} \sim \frac{g}{f\rho_0} \cdot \Delta\rho \cdot H^2 \quad . \tag{1}$$

Assuming that the advective-diffusive balance controls the stratification, the diapycnal flow scales as

$$\psi_{\mathrm{II}} \sim A \cdot \frac{\kappa}{H} \quad , \tag{2}$$

where A is the area of the low-latitude stratified part of the basin where the upwelling occurs. Note that in a more general case, where the globally integrated thermohaline circulation is considered, A should be interpreted as the effective area of the low-latitude upwelling in all ocean basins.

In a steady state the poleward and diapycnal flows must be equal, yielding the following relation between the pycnocline depth and the density difference:

$$H \sim \left(\frac{f\rho_0 A}{g}\right)^{1/3} \cdot \kappa^{1/3} \cdot \Delta\rho^{-1/3} \quad . \tag{3}$$

Substituting this result in Eq. (1) or (2) the steady-state overturning is obtained:

$$\psi \sim \left(\frac{gA^2}{f\rho_0}\right)^{1/3} \cdot \kappa^{2/3} \cdot \Delta\rho^{1/3} \quad , \tag{4}$$

which shows that the strength of the overturning is controlled by density as well as by vertical diffusivity.

2.1 Vertical mixing

The postulated physical basis of the vertical mixing, which controls the relation between diffusivity and density difference, plays an important role. A classical assumption concerning the vertical mixing is to keep the diffusivity fixed, viz. independent of the vertical stability. This parameterization, which is frequently used in ocean-circulation models, implies that the overturning scales as

$$\psi \sim \Delta\rho^{1/3} \quad . \tag{5}$$

The strength of the overturning is enhanced as the density difference increases, consonant with the established view (Park and Bryan, 2000). Note, however, that the response of the overturning to changes in $\Delta\rho$ is weaker than linear: according to Eq. (3), the pycnocline depth decreases with $\Delta\rho$ as $H \sim \Delta\rho^{-1/3}$, which, in view of Eq. (1), acts to curtail the overturning. An increase of $\Delta\rho$ yields not only stronger meridional velocities, but also a more shallow pycnocline, which inhibits the strengthening of the poleward transport.

Although κ frequently is assumed to be fixed in ocean modeling, straightforward energy considerations suggest that κ in fact depends on the vertical density difference (which is roughly proportional to the equator-to-pole density difference $\Delta\rho$). In a stratified fluid, small-scale vertical mixing (quantified in terms of κ) creates potential energy (Munk and Wunsch 1998) as

$$\mathcal{E} = \rho_0 \int \kappa N^2 \, \mathrm{d}z \quad , \tag{6}$$

where $\mathcal{E}$ is the rate of increase in potential energy per unit area and N the buoyancy frequency, defined by

$$N^2 = -\frac{g}{\rho_0}\frac{\partial\rho}{\partial z} \quad .$$

It is reasonable to assume that the rate of energy supply to small-scale mixing from, e.g., winds and tides is constant, which implies that also $\mathcal{E}$, the production rate of potential energy, should be constant. This argument, originally advanced by Phillips (1969), when applied to Eq. (6) yields the following dependence of the vertical diffusivity coefficient on the density difference:

$$\kappa \sim \frac{\mathcal{E}}{g\Delta\rho} \quad . \tag{7}$$

Thus, if the rate of energy supply available for small-scale vertical mixing is taken to be fixed, a stronger vertical density difference implies a smaller diffusivity. Using this result in Eq. (4) yields the overturning scales as

$$\psi \sim \Delta\rho^{-1/3} \quad . \tag{8}$$

As seen from Fig. 3, the two representations of mixing give rise to strikingly different overturning characteristics. If the diffusivity is constant, the overturning

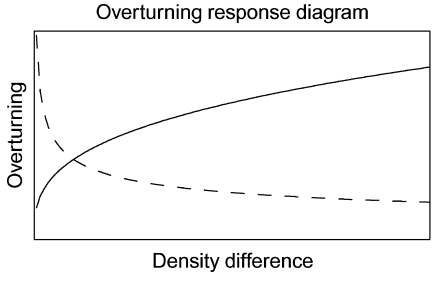

Fig. 3 Qualitative response diagram showing overturning as a function of the density difference between equator and pole for constant *solid* and stratification-dependent *dashed* diffusivity, respectively, according to the scale analysis (Eqs. 5 and 8)

intensifies with an increasing equator-to-pole density difference, whereas it weakens if the diffusivity is dependent on the vertical stability.

The pycnocline depth decreases with density difference ($H \sim \Delta\rho^{-2/3}$, cf. Eq. 3) more rapidly than in the previous case when the diffusivity was taken to be constant, having the somewhat counterintuitive consequence that the circulation slows down.

2.2 Effects of finite basin depth

For fixed mixing energy, the overturning increases beyond bounds when $\Delta\rho$ approaches zero (cf. Eq. 8). This raises the question whether the scale analysis is valid in the regime when the density difference is small.

According to Eq. (3), also the pycnocline depth becomes unbounded as $\Delta\rho$ approaches zero. As a result the pycnocline will eventually approach the bottom of the basin, $H \sim D$. When this occurs, the depth scale of the stratification is controlled by the geometry rather than by the advective-diffusive balance (Eq. 2), which becomes redundant, Hence the circulation is governed only by the thermal wind relation:

$$\psi \sim \frac{gD^2}{f\rho_0} \cdot \Delta\rho \ . \tag{9}$$

According to this result, the strength of the circulation responds in a linear fashion to changes in $\Delta\rho$. This result is independent of the representation of the diffusivity and is consequently valid for constant as well as stability-dependent diffusivity.

For fixed diffusivity, the response to changes of the density difference is weaker in the regime where $\Delta\rho$ is large ($H/D \ll 1$) than in the regime where it is small ($H \sim D$). Nevertheless, the derivative of the response has the same sign in both regimes. However, for fixed mixing energy the derivative changes sign between the regimes. The response is negative for large $\Delta\rho$, whereas it is positive for small $\Delta\rho$. Consequently, the strength of the circulation should assume a maximum for the specific density difference that yields $H \sim D$, which can be determined using Eq. (3):

$$\Delta\rho_m \sim \left(\frac{f\rho_0 A\mathcal{E}}{g^2}\right)^{1/2} \cdot D^{-3/2} \ .$$

Applying this result to Eq. (9) the maximum strength of the circulation is:

$$\psi_m \sim \left(\frac{A\mathcal{E}}{f\rho_0}\right)^{1/2} \cdot D^{1/2} \ .$$

Thus, the maximum possible overturning strength increases with the basin depth as well as with the rate of increase in potential energy due to mixing (i.e., $A\mathcal{E}$). However, it may be noted that ψ_m is not very sensitive to changes in these parameters; for instance, a doubling of D yields an increase in ψ_m of only about 40%.

3 The model

These results spurred us to investigate whether the two representations of the diffusivity yield similar results in an idealized numerical thermohaline circulation model. We use a zonally averaged, two-dimensional, thermohaline circulation model similar to the ones previously employed in various climate studies (Marotzke et al. 1988; Wright and Stocker, 1991), although the model domain in the present study is taken to encompass solely one hemisphere.

3.1 Governing equations

Essentially, the derivation of the zonally averaged model equations follows Marotzke et al. (1998). The model describes a Boussinesq fluid in hydrostatic equilibrium, confined within a basin of constant depth (D) and zonal width (B) that has the meridional length L. The horizontal momentum equation is

$$\gamma v = -\frac{1}{\rho_0}\frac{\partial p}{\partial y} \ , \tag{10}$$

where v is the zonally averaged meridional velocity, γ is a closure parameter relating flow speed and pressure gradient, ρ_0 is the reference density, p is the zonally averaged pressure, and y is the meridional coordinate. The basic closure hypothesis underlying Eq. (10) is that the east–west and the north–south pressure gradients are proportional (see, e.g. Wright et al., 1998 for an extensive discussion of flow representations in zonally averaged models). The hydrostatic balance is given by

$$\frac{\partial p}{\partial z} = -\rho g \ , \tag{11}$$

where ρ is the zonally averaged density and z is the vertical coordinate. Conservation of mass yields:

$$\frac{\partial v}{\partial y} + \frac{\partial w}{\partial z} = 0 \ , \tag{12}$$

where w is the zonally averaged vertical velocity. The conservation of heat and salt is given by

$$\frac{\partial}{\partial t}\begin{pmatrix} T \\ S \end{pmatrix} + v\frac{\partial}{\partial y}\begin{pmatrix} T \\ S \end{pmatrix} + w\frac{\partial}{\partial z}\begin{pmatrix} T \\ S \end{pmatrix} = \frac{\partial}{\partial z}\left[\kappa\frac{\partial}{\partial z}\begin{pmatrix} T \\ S \end{pmatrix}\right] \ , \tag{13}$$

where T and S are the zonally averaged temperature and salinity, respectively, and κ is the vertical diffusivity. For simplicity, a linear equation of state is used:

$$\rho(S,T) = \rho_0(1 - \alpha T + \beta S) \ , \tag{14}$$

where α and β are expansion coefficients for heat and salt, here taken to be constants. For this two-dimensional system it proves convenient to introduce a meridional streamfunction ψ:

$$Bv = -\frac{\partial \psi}{\partial z}, \qquad Bw = \frac{\partial \psi}{\partial y} \ ,$$

where ψ satisfies mass conservation (Eq. 12) and B is the zonal width of the basin.

By eliminating the pressure in the horizontal momentum balance (Eq. 10) and the hydrostatic balance (Eq. 11), rewriting the velocity in terms of the streamfunction, and, using the equation of state (Eq. 14), the following relation is obtained:

$$\frac{\partial^2 \psi}{\partial z^2} = -B \cdot \frac{g}{\gamma} \cdot \left(\beta \frac{\partial S}{\partial y} - \alpha \frac{\partial T}{\partial y} \right) \ . \tag{15}$$

This equation is used to calculate the streamfunction from temperature and salinity.

It is relevant to note that this zonally averaged model can be scaled using the same procedure as outlined in Section 2. If this is carried through, one finds that the pycnocline depth obeys

$$H \sim (\gamma \rho_0 L^2 / g)^{1/3} \cdot \kappa^{1/3} \cdot \Delta\rho^{-1/3} \ ,$$

and the overturning obeys

$$\psi \sim (g L^4 / \gamma \rho_0)^{1/3} \cdot (B/L) \cdot \kappa^{2/3} \cdot \Delta\rho^{1/3} \ .$$

The scale dependence of H and ψ on κ and $\Delta\rho$ derived in Section 2 thus also applies for the zonally averaged model, which is a consequence of the horizontal momentum closure (Eq. 10) employed here.

3.2 Boundary conditions

We are dealing with a basin of meridional extent L and depth D. No transport takes place through the solid boundaries, implying that $\psi = 0$ here. Neither heat nor salinity fluxes through the bottom are permitted, viz.

$$\frac{\partial T}{\partial z} = \frac{\partial S}{\partial z} = 0 \ .$$

At the surface the temperature is prescribed:

$$T_{\text{top}}(y) = \frac{\Delta T}{2} \cdot \left[1 + \cos\left(y \cdot \frac{\pi}{L} \right) \right] \ ,$$

where the temperature has a maximum ΔT at the equator and equals zero at the pole. The salinity is dynamically controlled through a prescribed salinity flux F at the surface:

$$F(y) = -F_0 \cdot \cos\left(y \cdot \frac{\pi}{L} \right) = -\kappa \frac{\partial S}{\partial z} \ ,$$

where F_0 is the magnitude of the maximum salinity flux. The physical interpretation of this prescribed distribution is that maximal net evaporation and precipitation take place at the equator and pole, respectively.

3.3 Parameterization of the diffusivity

The two different representations of mixing described above have been implemented for the model. In the first case κ is prescribed as a constant, κ_0, and is thus independent of the density stratification. In the second case κ is taken to be inversely proportional to $\overline{\Delta\rho}$ (cf. Eq. 7), which is the horizontal average of the top-to-bottom density difference. Specifically, κ has been given the form:

$$\kappa = \kappa_0 \cdot \frac{\Delta\rho_r}{\overline{\Delta\rho}} \ ,$$

where $\Delta\rho_r$ is a density difference used for reference purposes, and

$$\overline{\Delta\rho} = \frac{1}{L} \int_0^L (\rho_{\text{top}} - \rho_{\text{bottom}}) \, \mathrm{d}y \ ,$$

where the integrand is the vertical density difference between the surface and the bottom. In order to prevent too high κ values for weak density differences, an upper limit is set at $10 \cdot \kappa_0$.

3.4 Numerical procedures

Equation (13) is discretized using a leap-frog scheme and the calculations are initiated using Eulerian forward stepping. At each time step the streamfunction is calculated by integrating Eq. (15) twice. The spatial derivatives are discretized using centered differences. A staggered grid is employed, with the streamfunction in the corners and temperature and salinity at the center. The temperature and salinity resolutions are 51×41 in the horizontal and vertical direction, respectively.

In order to ensure numerical stability, horizontal diffusion, Asselin filtering, and horizontal three-point smoothing of the streamfunction are included in the computational scheme. The horizontal diffusivity constant is taken to be 160 $\text{m}^2\ \text{s}^{-1}$ and the Asselin time-filter constant is set to 0.1. Note that the horizontal diffusivity was taken to be as small as possible but yet large enough to suppress numerical noise and instability. The present diffusivity value should be so low that it has no significant effect on the large-scale flow. Convective adjustment following Yin and Sarachik (1994) has furthermore been incorporated to inhibit unstable stratification.

The fluid is initially at rest, at which time the temperature and salinity are taken to be constant in the basin. The time step used in the simulations is 12 h. The model is run until a steady state has been reached.

3.5 Reference state

We introduce a reference state that broadly corresponds to the present-day ocean, specified by the following parameters: $\Delta T_r = 25\ ^\circ\text{C}$, $\kappa_0 = 10^{-4}\ \text{m}^2\ \text{s}^{-1}$, $D = 3000$ m, $B = 6000$ km, $L = 6000$ km, $\alpha = 2 \times 10^{-4}\ ^\circ\text{C}^{-1}$, $\beta = 8 \times 10^{-4}$, $\gamma = 1.8 \cdot 10^{-3}\ \text{s}^{-1}$. Note that γ should be regarded as a tuning parameter, here adjusted so that the model yields ocean-like results for the parameter values introduced above. Note further that the freshwater forcing is zero in the reference state and that the

thermally induced equator-to-pole density difference, $\Delta\rho_r$, is 5 kg m^{-3}.

The reference state is the steady-state model solution that in the absence of freshwater forcing results from this parameter specification. In the reference state, the two mixing representations yield, by construction, an identical vertical diffusivity and consequently also identical model solutions. Figure 4 shows the temperature distribution as well as the streamfunction for this thermally forced reference state. The resulting circulation is of the forward, thermally dominated type, characterized by "narrow" sinking at high latitudes and "broad" upwelling at low latitudes. Note that the thermal stratification, with its well-defined thermocline, displays qualitative similarities with the real ocean.

It should be underlined that the reference state is characterized by a single nondimensional parameter:

$$\sigma = (\gamma\rho_0 L^2/g)^{1/3} \cdot \kappa^{1/3} \cdot \Delta\rho^{-1/3} \cdot D^{-1} \quad , \tag{16}$$

which controls the ratio between the thermocline depth and the basin depth. Provided that this parameter is chosen to yield a realistic thermocline depth, the actual strength of the overturning is basically irrelevant for the dynamics of the model.

To compare the present simulations with previous numerical and analytical investigations, it is useful to introduce a nondimensional measure of the freshwater forcing, which is here termed R. This parameter is defined as the ratio between the haline buoyancy flux, due to the surface salinity flux, and the thermal buoyancy flux associated with the simulated poleward heat transport in the reference state (say Q_r). The former buoyancy flux is given by $\beta F_0 BL/\pi$, which implies that

$$R = \frac{\beta F_0 BL c_p \rho_0}{\alpha Q_r \pi} \quad , \tag{17}$$

where c_p is the heat capacity of seawater. Note that it is F_0 that sets the strength of surface salinity flux and that $Q_r = 0.15$ PW.

It can be noted that the present tuning produces an overturning strength and a heat transport that are similar to those obtained from three-dimensional models in comparable geometry (see, e.g., Nilsson et al. 2003b). The observed northward heat transport in the Atlantic, on the other hand, is on the order of 1 PW. This discrepancy in heat transports is related to wind-driven circulation as well as to the fact that the real Atlantic receives thermocline water that has upwelled in the Indo-Pacific basin.

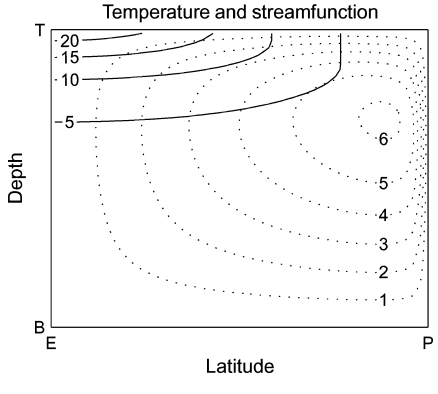

Fig. 4 Reference state temperature *solid lines* and streamfunction *dotted lines* in the basin at steady state, described in the text in Section 3.5. The *numbers* are given in. C and Sv and respectively. The x-axis is in the meridional direction and the y-axis in the vertical. E is the equator; P the pole; T the top; B the bottom

4 Results

Two types of numerical experiments are presented in what follows, those with only thermal forcing, and those where the circulation is forced by mixed boundary conditions. The thermal forcing is provided by the equator-to-pole surface temperature gradient, where the magnitude ΔT is changed for each simulation and the resulting steady state is subsequently examined. For the experiments with mixed boundary conditions, a fixed equator-to-pole temperature gradient, $\Delta T = \Delta T_r$, is applied, whereas R the strength of the freshwater forcing, is varied for each simulation.

4.1 Thermal forcing

When the system is subjected only to thermal forcing, the salinity is set to zero and thus density is a function of temperature only. The investigation has been carried through on the basis of a series of experiments with the forcing being increased for each simulation, whereafter the overturning strength at steady state has been measured. The magnitude of the forcing is given by ΔT and the strength of the steady-state overturning is measured by the maximum value of the streamfunction in a centrally located column, $\max_{z\in[0,D]}[\psi(y \sim L/2, z)]$.

Figure 5 shows the overturning strength as a function of the equator-to-pole temperature difference. In this

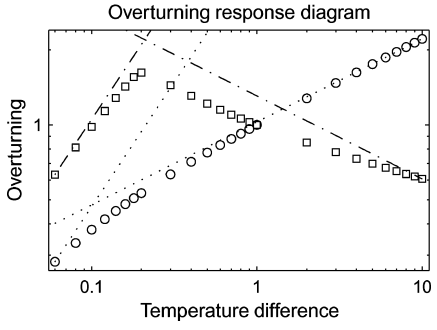

Fig. 5 Response of the overturning as function of equator-to-pole temperature difference, ΔT, for constant *circles* and stratification-dependent *squares* diffusivity, respectively. The flow is thermally forced and the overturning as well as the temperature difference is normalized at $\Delta T = \Delta T_r$. *Numbers* are nondimensional. *Dotted* and *dash-dotted lines* are results of the scale analysis for constant and stratification-dependent diffusivity, respectively (cf. Eqs. 5, 8, and 9). Axes are logarithmic

diagram the results from the numerical experiments, together with the relationships obtained from the scale analysis (Eq. 5, 8, and 9), are shown for the fixed as well as the stability-dependent diffusivity.

In the regime where the equator-to-pole temperature difference is sizable ($\Delta T \geq 5$ °C), there is a qualitative difference between the overturning response for the two different diffusivity parameterizations. In agreement with the scale-analysis results (cf. Eq. 5 and 8), the strength of the overturning intensifies with equator-to-pole temperature difference using the constant-diffusivity parameterization, whereas it becomes weaker for the stability-dependent diffusivity parameterization.

This may be contrasted with the behavior in the regime where the equator-to-pole temperature difference is small ($\Delta T \leq 5$ °C). Here, the overturning strength increases with the temperature difference for both diffusivity representations. Consonant with the scale-analysis results (cf. Eq. 9), the overturning strength is essentially proportional to the density contrast.

According to the theoretical considerations, the response of the overturning is intimately related to the response of the thermocline depth, given as $H \sim \Delta T^{-1/3}$ and $H \sim \Delta T^{-2/3}$, respectively, for the two different diffusivity representations (cf. Eq. 3). In order to investigate how the thermocline depth varies with temperature difference in the model, a thermocline depth index H_T is defined as

$$H_T = \int_{-D}^{0} \frac{T(z) - T_{\mathrm{bottom}}}{T_{\mathrm{top}} - T_{\mathrm{bottom}}} \, \mathrm{d}z \ , \tag{18}$$

where T_{top} and T_{bottom} are the temperature at the surface and bottom, respectively.

The variation of thermocline depth with temperature difference is shown in Fig. 6. The variation of H_T in the model follows the predictions of the scale analysis in the regime where $\Delta T \geq 5$ °C. In the region where $\Delta T \leq 5$ °C the thermocline depth index saturates close to 0.5, implying that the thermocline effectively has reached the bottom ($H \sim D$).

The overturning response in Fig. 5 and the thermocline depth response in Fig. 6 (shown for data from a column near the center of the basin) proved to be uniformly valid in the greater part of the basin. The exception is the region poleward of the global maximum of the streamfunction where downwelling occurs.

4.2 Mixed boundary conditions

After noting the different responses depending on the representation of the diffusivity, it is of interest to analyze how freshwater forcing affects the circulation. The density is now a function of temperature as well as salinity, and consequently the salinity-flux and temperature-boundary conditions jointly force the circulation. Note that, in contrast to the case when only thermal forcing is applied, the equator-to-pole surface density difference is not prescribed but dynamically determined by the flux condition at the surface. The thermal forcing is taken to be constant, but the intensity of the freshwater forcing is slightly varied between each simulation. In what follows the thermally dominated forward circulations are first analyzed, whereafter salinity-dominated, reversed circulations are dealt with separately. The steady state at $R = 0$ is identical to that obtained for the thermally forced simulation at $\Delta T = \Delta T_r$.

Figure 7 shows the resulting strength of the streamfunction (defined above) as a function of the freshwater forcing. When the strength of the freshwater forcing is increased, the circulation weakens for the constant-diffusivity case. The opposite is true when the stability-dependent diffusivity parameterization is used: a stronger freshwater forcing is now associated with a strong overturning. This is in broad agreement with the results from the thermally forced simulations (cf. Fig. 5). As the freshwater forcing is increased, the salinity contrast is magnified, implying that the equator-to-pole density difference weakens. This corresponds to a weaker

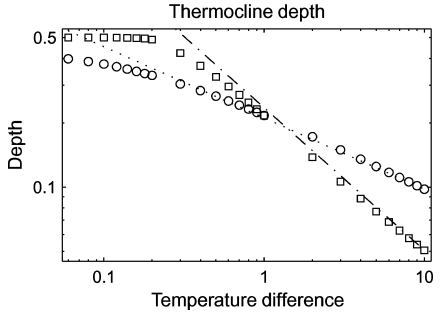

Fig. 6 Thermocline depth index (cf. Eq. 18) for constant *circles* and stratification-dependent *squares* diffusivity. The flow is thermally forced. Thermocline depth index for a column in the center of the basin as a function of equator-to-pole temperature difference. The depth index is normalized with the basin depth D and the temperature difference with ΔT_r. *Numbers* are nondimensional. *Dotted lines* and *dash-dotted lines* are results from the scale analysis for constant and stratification dependent diffusivity, respectively. *Axes* are logarithmic

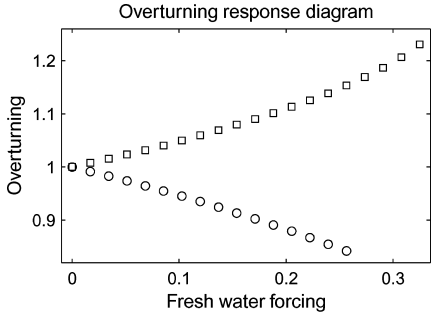

Fig. 7 Response diagram of the overturning as function of the strength of the freshwater forcing, R, for constant *circles* and stratification-dependent *squares* diffusivity, respectively. Heat and freshwater force the circulation. The overturning is normalized at $R = 0$. *Numbers* are nondimensional

equator-to-pole temperature difference in the simulations using only thermal forcing.

It should be emphasized that no steady forward circulations are found when $R > 0.33$. The underlying reason has to do with feedbacks between the circulation and the salinity fields, an issue which deserves discussion. In the case with only thermal forcing there is a negative feedback between the temperature difference and the heat flux since a greater temperature difference results in an enhanced heat flux, independent of the diffusivity representation. The existence of solely a negative feedback implies that there is one single stable equilibrium state for each ΔT. However, the freshwater forcing introduces an additional feedback mechanism which makes the dynamics more complex.

To begin with, it should be recognized that the freshwater forcing acts to increase the equator-to-pole salinity contrast, regardless of the magnitude of the salinity contrast. In a steady state the advective salinity flux is the only mechanism capable of balancing the freshwater forcing. The feedback between the salinity difference and the advective salinity flux determines the stability of the system when it departs from a steady state. The essentials of this feedback are contained in the linearized evolution of a small perturbation on the basic equator-to-pole salinity contrast $\overline{\Delta S}$, as the following schematic relation describes:

$$\frac{\mathrm{d}\Delta S'}{\mathrm{d}t} \propto -\Delta S' \cdot \overline{\psi} - \overline{\Delta S} \cdot \psi' \ ,$$

where overbars denote basic-state quantities and primes denote perturbations. The first r.h.s. term represents how the basic-state flow affects a perturbation in the salinity contrast. This part of the feedback is independent of the relation between density and circulation and is hence also independent of the diffusivity representation. It is negative definite, since the advection counteracts the salinity perturbation. The second r.h.s. term describes the interaction between a flow perturbation and the basic salinity contrast. This feedback depends on the relation between density difference and circulation. For constant diffusivity, as well as in the classical box model due to Stommel (1961), a positive perturbation in the salinity contrast gives rise to a decrease of the advection (relative the basic state). This will amplify the initial perturbation in the salinity contrast, hereby making this part of the feedback positive. Thus, the two feedback components counteract each other and the net feedback can be negative as well as positive. For the stability-dependent diffusivity, on the other hand, a positive perturbation in the salinity contrast implies an enhanced circulation. This will dampen out the salinity perturbation (implying that the second r.h.s. term constitutes a negative feedback). Hence, the total feedback is always negative.

Can these theoretical considerations serve to illuminate the model results? For the case when $\psi \sim \Delta\rho^{1/3}$ (corresponding to fixed diffusivity) and when the freshwater forcing is weak, the negative component of the feedback predominates. However, it weakens as the freshwater forcing becomes stronger and the salt contrast builds up, whereas the positive part of the feedback becomes stronger. Freshwater forcing consequently destabilizes the circulation. At some stage the positive part of the feedback overwhelms the negative one and the system becomes unstable. Thus, there is no stable forward circulation when the freshwater forcing is stronger, but a reversed circulation is possible (a topic to be dealt with below). This behavior of the feedback proves to be qualitatively the same as in Stommel's model (Stommel 1961). The present discussion suggests that the numerical model with fixed diffusivity yields an overturning that weakens with the density contrast up to a point where a forward circulation cannot be found. Instead, a steady-state reversed circulation is obtained.

For stability-dependent diffusivity ($\psi \sim \Delta\rho^{-1/3}$) the response should be fundamentally different, since the feedback is always negative. In the absence of a positive feedback the system should be stable, independent of the strength of the freshwater forcing, i.e., no threshold levels should exist. Furthermore, salinity perturbations should be attenuated more rapidly when the freshwater forcing is strong. However, this is not the case in the numerical simulations. For $R > 0.33$ the model does not attain stable steady states but oscillating transient states. When attempting to explain why the model does not comply with the theoretical considerations, the effects of a finite basin depth could be relevant. According to the scale analysis, a bottom influence could reverse the relation between flow and density difference (cf. Sect. 2.2). The pycnocline depth (not shown here) increases with freshwater forcing but has not reached the bottom when the forward circulation breaks down. At this stage $H_\rho < 0.3$, where H_ρ is defined similarly as H_T with temperature replaced by density. Thus bottom effects can be ruled out. A more probable explanation is that the scale analysis applies only in the region where upwelling occurs, i.e., equatorwards of the global maximum of the streamfunction.

Figure 8 shows the meridional variation of the maximum of the streamfunction. Equatorwards of the global

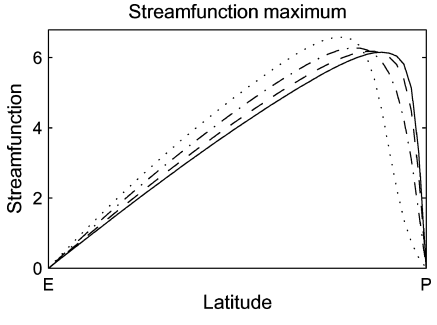

Fig. 8 The meridional variation of the maximum of the streamfunction in each column with different freshwater forcings using stratification-dependent diffusivity. The *solid line* shows the maximum of the streamfunction for no freshwater forcing ($R = 0$), the *dashed line* for $R = 0.10$, the *dash-dotted* for $R = 0.22$ and the *dotted* for $R = 0.32$. *Numbers* are given in Sv. The x-axis is in the meridional direction.; E is the equator and P the pole

maximum the streamfunction increases with the freshwater forcing while it decreases poleward of the global maximum. Thus, the discussion of feedbacks above does not apply in the poleward region. Here the feedback between salinity difference and advective salinity flux may well become positive. In fact, in the simulation where the forward circulation broke down (at $R = 0.33$), a salinity perturbation developed at high latitudes. As time progressed this perturbation grew in magnitude and extent. As a result, the cell of forward circulation receded equatorwards and vanished temporarily to be replaced by a reversed circulation. Eventually a quasiperiodic state was attained (discussed below).

Finally, it is worth mentioning that the dependence of maximum heat flux on the freshwater forcing is similar to that of the overturning (cf. Fig. 7). Thus for constant diffusivity, the heat flux decreases with freshwater forcing, a dependence which is well established. A somewhat peculiar effect is that for the fixed-energy parameterization, the heat flux increases with freshwater forcing. Hence it is possible to maintain a strong heat flux for a weak density contrast.

4.3 Time dependence

It was noted above that when the freshwater forcing exceeded $R = 0.33$, no steady-state solutions with forward circulation were obtained when the model had stability-dependent vertical mixing. For stronger freshwater forcing, the flow exhibited pronounced time dependence. Although this issue lies outside the main focus of the present study, the dynamics of the time-dependent states warrant a brief comment. Consider to begin with Fig. 9a, which shows the time evolution of the streamfunction at the center of the basin (for $R = 0.33$). As illustrated, the flow undergoes a quasiperiodic oscillation, alternating between a strong forward circulation and a weak reversed circulation. By inspecting the distribution of ψ in two of the extreme phases of the oscillation (see Fig. 9b and c), the following picture emerges. In the phase of weak flow at the center of the basin, there are two distinct circulation cells: forward flow occurs in the southern domain, whereas the northern domain is characterized by a weak reversed circulation. Formation of rather warm and saline deep water occurs between the two cells. In phases of strong flow, the forward circulation occupies the bulk of the basin. Here, broad down welling occurs in the northern half of the basin. Thus, the oscillation brings the system from an essentially thermally dominated forward state to a hybrid state with partly reversed flow, and back again. Throughout the cycle, the haline- and thermal-density contributions are comparable in the northern part of the basin, which causes the density contrast to be weak in this region.

The oscillation described here kinematically resembles the "thermohaline flushings" that have been reported from several studies based on three-dimensional ocean models (e.g., Weaver et al. 1993). As in a typical cycle of thermohaline flushing, the present model produces relatively long dormant periods, followed by short bursts of intense forward circulation. It should be stressed, however, that the stability-dependent vertical mixing is crucial for the oscillations in our two-dimensional model; only steady equilibria are found when a constant vertical diffusivity is employed. Three-dimensional models, on the other hand, produce flushing cycles when the vertical diffusivity is taken to be fixed, as exemplified by the study of Weaver et al. (1993).

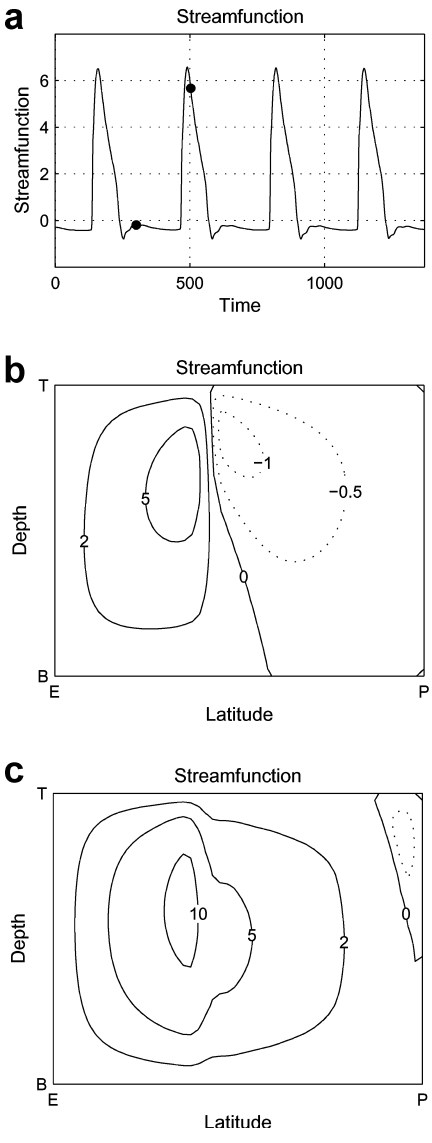

Fig. 9 Transient streamfunction **a** Streamfunction at the center of the basin as a function of time with freshwater forcing at $R = 0.33$ using stratification-dependent diffusivity. The *bullets* mark the weak and strong phases shown in **b** and **c**, respectively. *Numbers* are given in Sv and years, respectively. **b** Streamfunction at the weak phase at $t = 301$ years with freshwater forcing at $R = 0.33$ using stratification-dependent diffusivity. *Numbers* in Sv. *Solid contour lines* correspond to positive values and *dotted* to negative. The x-axis is in the meridional direction and the y-axis in the vertical. E is the equator; P the pole: T the top, B bottom **c** As **b** but at strong phase at $t = 503$ years

4.4 Reversed circulation

When the salinity field dominates the density distribution, the flow and the equator-to-pole density gradient become reversed. In this regime, narrow sinking occurs in low latitudes, which is compensated by broad upwelling over the rest of the basin. As the stratification is controlled by salinity, a stronger freshwater forcing now implies a more pronounced density difference. Essentially, this is the opposite of the state of affairs in the thermally dominated regime with forward circulation.

Figure 10 provides an overview of all steady states that have been obtained in the numerical investigation. The figure also indicates the predictions from the conceptual model of Nilsson and Walin (2001) (illustrated by the dotted lines). Consider first the reversed flow obtained when the model has constant diffusivity. As for the forward circulation, a stronger density difference implies a stronger circulation. Accordingly, the increase in circulation with increasing freshwater forcing, illustrated in Fig. 10, is expected. It is worth noting that the predictions from Nilsson and Walin (2001) describe reasonably accurately the forward as well as the reversed circulation in this case. Note further that no effort has been made to obtain reversed flow for weak freshwater forcing.

It proved more challenging to obtain stationary reversed flows when the stability-dependent mixing was employed. However, after extended numerical integrations a few equilibria were obtained. Figure 10 shows that the reversed circulation slows down when the freshwater forcing increases. This behavior is analogous to the dynamics in the forward regime: a stronger freshwater forcing yields an enhanced (salinity-dominated) density contrast. This implies reduced vertical mixing, which causes the thermocline depth to decrease to such an extent that the overturning slows down, despite an increased equator-to-pole density difference. As evident from Fig. 10, in this case the numerically simulated reversed circulation only qualitatively follows the conceptual model of Nilsson and Walin (2001). It is nevertheless of interest to note that the conceptual model predicts a threshold freshwater forcing, below which steady reversed circulation should be possible. The reason is that there now is a positive feedback between perturbations in salinity and circulation: a weaker salinity contrast yields a stronger flow, which in turn further reduces the salinity contrast. Thus, it is essentially the same mechanism that destabilized the forward circulation when the vertical diffusivity is fixed.

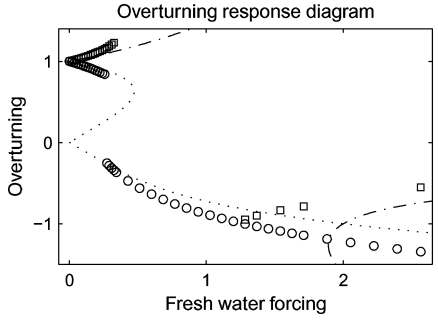

Fig. 10 Response of the overturning as function of the strength of the freshwater forcing, R, for constant *circles* and stratification-dependent *squares* diffusivity, respectively. Heat and freshwater forces the circulation. *Dotted* and *dash-dotted lines* lines are predictions from the conceptual model of Nilsson and Walin (2001) for constant and stratification-dependent diffusivity, respectively. The overturning is normalized at $R = 0$. *Numbers* are nondimensional

5 Discussion

In our two-dimensional numerical model, the nature of the vertical mixing proved to be crucial for the response of the circulation to changes in the surface fluxes of heat and freshwater. When the vertical mixing was represented by a fixed vertical diffusivity, the forward circulation increased with increasing equator-to-pole density difference. This is the generally anticipated behavior, which has been reproduced in many numerical investigations (e.g., Park and Bryan 2000). In contrast, when the vertical diffusivity decreased with stratification (at a rate that implied a fixed mixing energy) the opposite result was obtained: a weaker density difference yielded a stronger forward circulation.

This qualitative difference in the response of the circulation was encountered in the simulations with only thermal forcing as well as in those with mixed boundary conditions. For the stratification-dependent mixing, the forward circulation intensified with increasing freshwater forcing. To our knowledge, this remarkable thermohaline response has not been reported from previous numerical investigations. A closer inspection of these simulations revealed that while the flow intensified in the bulk of the basin, it slowed down at high latitudes. The local freshwater hampering of the high-latitude circulation eventually destabilized the steady forward equilibrium, despite stronger freshwater forcing serving to augment the circulation in the greater part of the basin. However, the branch of thermally dominated steady states was not succeeded by a salinity-dominated branch with reversed circulation (as was the case when a fixed diffusivity was employed). Rather, quasiperiodic flows resulted, which oscillated between phases of forward circulation of varying spatial extent and strength. It is interesting to note that the conceptual model due to Nilsson and Walin (2001) describes the simulated response of the forward circulation to freshwater forcing rather well for both mixing representations; see Fig. 10. However, the predictions of this model concerning the stability of the forward circulation proved to be less applicable to our numerical simulations. According to the conceptual two-layer model, the forward circulation should remain stable until the freshwater forcing is so strong that the pycnocline approaches the sea floor when stability-dependent mixing is employed. The forward

circulation in the numerical model broke down well before that stage was reached. The most likely explanation is that the two-layer model, although relevant for steady-state flows, does not resolve the spatial structure of the perturbations destabilizing the numerical model.

Are the results from this idealized study of relevance for the thermohaline circulation in the real ocean? To approach this question, it must be recognized that our knowledge of the vertical mixing in the ocean interior is far from complete (e.g., Toole and McDougall 2001). Currently it is not known with any degree of precision how the turbulent vertical diffusivity would change in response to an altered vertical stratification in the World Ocean. Keeping this basic difficulty in mind, it is thus most relevant to ask whether the thermohaline circulation in more realistic models would be as sensitive to the nature of vertical mixing as it proved to be in our one-hemisphere zonally averaged model. To begin with, it can be stated that our model produces relations between the prescribed equator-to-pole temperature difference and the overturning strength that are similar to those obtained by Nilsson et al. (2003b), who studied one-hemisphere flows using a three-dimensional model. Accordingly, for the purely thermally forced flows, the present zonally averaged model seems to give a reasonable description of the meridional overturning dynamics.

5.1 Relevance for two-hemisphere flows

The use of a one-hemisphere basin is an obvious limitation and motivates a comment on the relevance of our results for thermohaline flows in a two-hemisphere basin. Focusing on thermally forced flows, it can be noted that the studies by Klinger and Marotzke (1999) and Marotzke and Klinger (2000) demonstrate that even a weak pole-to-pole temperature (i.e., density) difference yields a flow that is strongly asymmetric with respect to the equator. Obviously, the present theoretical and numerical considerations provide no information on the dynamics controlling the asymmetry of these two-hemisphere flows. However, Klinger and Marotzke (1999) noted that the thermocline depth and the net overturning (i.e., the combined sinking in the two hemispheres) of the asymmetric flows scaled essentially as in the one-hemisphere case: in their simulations (where a fixed diffusivity was employed) the net overturning followed roughly $\Delta T^{1/3}$, where ΔT represented the largest equator-to-pole temperature difference (i.e., characterizing the hemisphere where the bulk of the sinking occurred). Based on the results of Klinger and Marotzke, it seems plausible that the present results apply qualitatively also for the net overturning of an asymmetric two-hemisphere flow, which essentially should be controlled by the basin-averaged vertical diffusivity and the maximum density contrast.

In the simulations with mixed boundary conditions, the one-hemisphere geometry introduces an additional problem: it excludes the possibility of equatorially asymmetric perturbations, which have a destabilizing influence on the symmetric thermally dominated circulation in a two-hemisphere basin (Weijer and Dijkstra 2001; Nilsson et al. 2003a). It is well established that in a two-hemisphere basin the thermohaline circulation tends to attain an equatorially asymmetric state, rather than a state of reversed circulation, as the freshwater forcing is increased (Marotzke et al. 1988; Thual and McWilliams 1992; Klinger and Marotzke 1999). Welander (1986) suggested that the asymmetric thermohaline circulation conceptually can be viewed as a hybrid state, with thermal dominance in one hemisphere and haline dominance in the other. This idealized picture may suggest that our results concerning the effect of vertical mixing on the circulation in the forward and reversed regimes, respectively, can be translated to asymmetric circulations in a two-hemisphere system. However, this is probably misleading, as there tends to be an element of pole-to-pole circulation in the asymmetric regime, rather than two independent cells with different directions of flow (e.g., Klinger and Marotzke 1999). Accordingly, the effect of a coupling between mixing and stratification on asymmetric two-hemisphere thermohaline circulation warrants further study.

5.2 Concluding remarks

It must further be emphasized that in our one-hemisphere model, the production and sinking of dense water must be balanced by the upwelling sustained by vertical mixing in the ocean interior. In the World Ocean, however, the wind directly forces upwelling in the Southern Ocean (Toggweiler and Samuels 1995; Rahmstorf and England 1997), where the surface Ekman drift carries cold water equatorwards. In fact, results from the conceptual model of Saenko and Weaver (2003) suggest that the overturning strength in the real ocean is probably less sensitive to the equator-to-pole density difference and the nature of vertical mixing than it is in our idealized one-hemisphere model; if the wind-forced Southern Ocean upwelling is fixed, it provides a baseline for the strength of the global overturning.

Furthermore, it should be underlined that our results concern the steady-state response of the thermohaline circulation to variations in the freshwater forcing. In the context of climate change – past as well as future – it may rather be the response of the thermohaline circulation to transient and abrupt changes of the surface forcing that matters. This transient type of response is of immediate relevance for how the thermohaline circulation will respond to future global warming (see, e.g., Rahmstorf 2000; Marotzke 2000). In this context it is interesting to mention a recent coupled ocean–atmosphere study concerning the sensitivity of the Atlantic thermohaline circulation reported by Otterå et al. (2003). Starting from present-day climatic conditions, they introduced a strong freshwater perturbation in the northern North Atlantic 0.2 Sv kept constant). Initially,

the Atlantic thermohaline circulation declined; however, after some 50 years the circulation started to regain strength and eventually stabilized. In the ocean model, Otterå et al. employed a stability-dependent vertical mixing. Based on analyses of the model result, they concluded that enhanced vertical mixing played an important role for the stabilization of the Atlantic circulation. Thus, it seems highly motivated to further explore to what extent the nature of vertical mixing may affect the dynamics of the thermohaline circulation.

Acknowledgements This work was supported by the Swedish National Space Board and the Swedish Research Council. We would like to thank Professor Peter Lundberg for discussions and valuable comments. We would also like to thank two anonymous reviewers for their constructive suggestions.

References

Huang RX (1999) Mixing and energetics of the oceanic thermohaline circulation. J Phys Oceanogr 29(4): 727–746

Kato H, Phillips OM (1969) On the penetration of a turbulent layer into a stratified fluid. J Fluid Mech 37: 643–655

Klinger BA, Marotzke J (1999) Behavior of double-hemisphere thermohaline flows in a single basin. J Phys Oceanogr 29(3): 382–399

Levitus S (1982) Climatological atlas of the world ocean. NOAA Professional paper (13): 173 pp

Lyle M (1997) Could early cenozoic thermohaline circulation have warmed the poles? Paleoceanography 12(2): 161–167

Marotzke J (2000) Abrupt climate change and thermohaline circulation: mechanisms and predictability. Proceedings of the National Academy of Sciences (USA) 97: 1347–1350

Marotzke J, Welander P, Willebrand J (1988) Instability and multiple steady states in a meridional-plane model of the thermohaline circulation. Tellus, Ser A 40(2): 162–172

Marotzke J, Klinger BA (2000) The dynamics of equatorially asymmetric thermohaline circulations. J Phys Oceanogr 30(5): 955–970

Munk WH (1966) Abyssal recipes. Deep-Sea Res 13: 707–730

Munk WH, Wunsch C (1998) Abyssal recipes II: energetics of tidal and wind mixing. Deep-Sea Res Part I 45(12): 1977–2010

Nilsson J, Walin G (2001) Freshwater forcing as a booster of thermohaline circulation. Tellus Series A 53(5): 628–640

Nilsson J, Broström G, Walin G (2003a) On the spontaneous transition to asymmetric thermohaline circulation. Tellus (in press)

Nilsson J, Broström G, Walin G (2003b) The thermohaline circulation and vertical mixing: Does weaker density stratification give stronger overturning. J. Phy Oceanogr 33(12): 2781–2795

OtteråOH, Drange H, Bentsen M, Kvamstø NG, Jiang D (2003) The sensitivity of the present-day atlantic meridional overturning circulation to freshwater forcing. Geophys Res Lett 30(17): 1898

Park Y-G, Bryan K (2000) Comparison of thermally driven circulations from a depth-coordinate model and an isopycnal-layer model, part I. Scaling-law sensitivity to vertical diffusivity. J Phys Oceanogr 30(3): 590–605

Rahmstorf S (2000) The thermohaline ocean circulation: a system with dangerous thresholds? Clim Change 46(3): 247–256

Rahmstorf S, England MH (1997) Influence of southern hemisphere winds on north atlantic deep water flow. J Phys Oceanogr 27(9): 2040–2054

Saenko OA, Weaver AJ (2003) Southern Ocean upwelling and eddies: sensitivity of the global overturning to the surface density range. Tellus Series A 55(1): 106–111

Stommel H (1961) Thermohaline convection with two stable regimes of flow. Tellus 13(2): 224–230

Thual O, McWilliams JC (1992) The catastrophe structure of thermohaline convection in a two-dimensional fluid model and comparison with low-order box models. Geophys Astrophys Fluid Dynam 64(1–4): 67–95

Toggweiler JR, Samuels B (1995) Effect of drake passage on the global thermohaline circulation. Deep-Sea Res part I 42(4): 477–500

Toole JM, McDougall TJ (2001) Mixing and stirring in the ocean interior. In: Siedler G, Church J, Gould J (eds) Ocean circulation and climate, vol 77. Academic Press pp 337–356

Weaver AJ, Marotzke J, Cummins PF, Sarachik ES (1993) Stability and variability of the thermohaline circulation. J Phys Oceanogr 23(1): 39–60

Weijer W, Dijkstra HA (2001) A bifurcation study of the three-dimensional thermohaline ocean circulation: the double hemispheric case. J Mar Res 59(4): 599–631

Welander P (1986) Thermohaline effects in the ocean circulation and related simple models. In: Willebrand J, Anderson DLT (eds) Large-scale transport processes in oceans and atmosphere. D. Reidel, New York, pp 163–200

Wright DG, Stocker TF (1991) A zonally averaged ocean model for the thermohaline circulation, part I. Model development and flow dynamics. J Phys Oceanogr 21(12): 1713–1724

Wright DG, Stocker TF, Mercer D (1998) Closures used in zonally averaged ocean models. J Phys Oceanogr 28(5): 791–804

Yin FL, Sarachik ES (1994) An efficient convective adjustment scheme for ocean general circulation models. J Phys Oceanogr 24(6): 1425–1430